CHAPTER 6

6.0 CHAR GASIFICATION WITH CARBON DIOXIDE: KINETIC MODELLING AND PARAMETERS EVALUATION

6.1 Introduction

The main objective of kinetic modelling is to use fundamental equations to predict the gasification reaction process (Murillo *et al*., 2004; Zhang *et al*., 2010). The kinetic modelling, as well as the evaluation of various kinetic parameters, is presented in this chapter. A kinetic model, the random pore model (RPM), was chosen amongst other models to adequately model the char-CO_2 gasification reaction. The choice was based

on fundamental principles and relevance to this type of heterogeneous reaction. The model description is given in Sections 6.2 and 6.3, while the evaluation of the kinetic parameters and the modelling and validation of the experimental results is presented in Sections 6.5 and 6.6 respectively.

6.2 The Random Pore Model

The random pore model and its modifications have been used by several investigators in the modelling of heterogeneous char-CO_2 gasification reactions (Gavalas, 1980; Bhatia and Perlmutter, 1980 and 1981; Radovic *et al*., 1985; Miura *et al*., 1990; Ochoa *et al*., 2001; Murillo *et al*., 2004 and 2006; Kajitani *et al*., 2006; Zhang *et al*., 2006; Kaitano, 2007; Everson *et al*., 2008a; Sangtong-Ngam and Narasingha 2008).

The basic assumptions and features of the random pore model are as follows:

- The random pore model was developed on the assumption that the reaction sites occur in cylindrical pores of arbitrary pore size distribution, which may also overlap, as they grow or collapse during reaction.

- The RPM encompasses the intra-particle reaction, which arises due to the changes imparted to the char (change in porosity, surface area, morphology, etc) by devolatilisation, thermal annealing and cracking. These cannot be neglected, as the resultant char physical and chemical properties impact on the overall reaction and overcome the limitations usually experienced with the use of the unreacted shrinking core model.

- The changes in surface area during reaction are also accounted for in terms of the initial surface area and other structural properties of the reacting char. Thus, the variations of the active surface area of the char as gasification progresses are accounted for by the random pore model.

- The model can also be used to identify the different reaction regimes by considering limiting values for dimensionless groups characteristic of the different controlling mechanisms.

- The random pore model is more flexible than the other models as it is capable of describing processes that show a maximum rate at certain conversion levels, as well as processes that do not exhibit this behavior.

6.3 The Random Pore Model Equation

The experimental conditions as given in Table 4.3, Section 4.4, and the very long experimental burnout times, were such that the char-CO_2 gasification reactions were considered to be under the chemical reaction kinetics controlled regime (Regime I). Furthermore, these conditions were similar to conditions used by various investigators for Regime I char-CO_2 gasification kinetics (Dutta *et al*., 1977; Radovic *et al*., 1985; Matsui *et al*., 1987; Hampartsoumian *et al*., 1993; Fu and Wang, 2001; Ochoa *et al*., 2001; Sinağ *et al*., 2003; Kajitani *et al*., 2006; Zhang *et al*., 2006; Everson *et al*., 2006). Thus, random pore model (RPM) evaluations were based on Regime I as modified by Everson *et al*. (2008a).

According to Bhatia and Perlmutter (1980), the RPM overall reaction rate can be described as:

$$\frac{dX}{dt} = \frac{r_s S_o (1-X)\sqrt{1-\psi \ln(1-X)}}{(1-\varepsilon_o)} \tag{6.1}$$

The influence of the operating variables are taken care of by the inclusion of the intrinsic reaction rate, r_s, in the overall reaction rate equation, while variations in structural properties are compensated for by the structural parameter, ψ, defined as a function of the initial char properties:

$$\psi = \frac{4\pi L_o (1-\varepsilon_o)}{S_o^2} \tag{6.2}$$

By introducing a dimensionless parameter, τ, defined by Kaitano (2007) and Everson *et al*. (2008a) as:

$$\tau = \frac{r_s S_o t}{(1-\varepsilon_o)} \tag{6.3}$$

Equation 6.1 can be rewritten in a dimensionless form:

$$\frac{dX}{d\tau} = (1-X)\sqrt{1-\psi \ln(1-X)} \tag{6.4}$$

Integration of Equation 6.4 gives the carbon conversion, *X*, as a function of time, *t*, or the dimensionless time, τ (implicit and explicit).

$$t = \frac{2(1-\varepsilon_o)}{r_s S_o \psi}\left(\sqrt{1-\psi \ln(1-X)} - 1\right) \tag{6.5}$$

Substituting the dimensionless parameter, τ, defined in Equation 6.3, into Equation 6.5 yields the following:

$$\tau = \frac{2}{\psi}\left(\sqrt{1-X\psi \ln(1-X} - 1\right) \tag{6.6}$$

Rearranging Equation 6.6 and expressing the carbon conversion, *X*, as a function of the dimensionless time, τ , gives the model equation:

$$X = 1-\exp\left[-\tau\left(1+\frac{\psi\tau}{4}\right)\right] \tag{6.7}$$

The model equation described in Equation 6.7 can be simplified by incorporating into it, a time factor, t_f, defined as (Everson *et al*., 2008a):

$$t_f = \frac{r_s S_o}{(1-\varepsilon_o)} \tag{6.8}$$

Expressing Equation 6.7 in terms of the time factor, t_f, and the real time, *t*:

$$X = 1 - \exp\left[-t_f t \cdot \left(1 + \frac{t_f t \psi}{4}\right)\right] \tag{6.9}$$

To further simplify the use of the model equations, Kaitano (2007) and Everson *et al*. (2008) proposed the use of the reduced time, (t/t_x), in place of real time, t, in Equation 6.5.

The ratio of the reaction time and time for a fractional conversion of *X*, (t/t_x), is independent of the parameters before the square root term in Equation 6.5, except the structural parameter, ψ. This will have the effect that all results for a particular gasified char should be the same, thereby simplifying the determination of the structural parameter numerically. Equation 6.5 thus takes the form:

$$\frac{t}{t_{0.9}} = \frac{\sqrt{1 - \psi \ln(1 - X)} - 1}{\sqrt{1 - \psi \ln(1 - 0.9)} - 1} \tag{6.10}$$

where $t_{0.9}$ is the time for 90% carbon conversion of the char (carbon). It should however be noted that:

$$\frac{t}{t_{0.9}} = \frac{\tau}{\tau_{0.9}} \tag{6.11}$$

Since the char-CO_2 gasification reaction follow Arrhenius type kinetics with dependency on temperature and the power rate law, the intrinsic reaction rate, r_s, equation was based on the nth order power rate relationship. This is expressed as:

$$r_s = k_{so} \exp\left(\frac{-E_a}{RT}\right) y_{CO_2}^m \tag{6.12}$$

6.4 Validation Procedure

The use of the random pore model to determine the kinetic parameters under the chemical reaction controlled regime (Regime 1) requires that the structural parameter, ψ, and the time factor, t_f, be evaluated. Kaitano (2007) noted that the structural parameter can be determined either from BET results or from image analysis results as proposed by Bhatia and Perlmutter (1980), or from experimental data (Liu *et al*., 2000).

The limitation of these methods is that the surface area and pore volume approximations using BET and image analyses results of heterogeneous coal particles with non-uniform pore sizes are not precise. This arises due to the estimations required in the description of the non-uniform pore sizes especially the micropores (Kaitano, 2007). The assumptions used in image analysis may introduce some ambiguities as well. The maximum of the experimental reaction rate curves obtained from the conversion-time profiles had been used to determine the structural parameter (Liu *et al*., 2000). The method of Liu and co-workers (2000), involves the numerical differentiation of the experimental data, which could be subject to errors as a result of the chosen differential intervals as noted by Kaitano (2007).

These shortcomings were overcome in this investigation by evaluating the structural parameter using Equation 6.10 and involves fitting the equation by regression with an arbitrary structural parameter to corresponding experimental result. The regressed ψ-value that gives the best fit is accepted as the structural parameter for the experiment and repeated for all the experiments. The validity of the regressed structural parameter is further verified by plotting the reduced time against carbon conversion up to 90% conversion. This plot is supposed to be the same for any of the four chars for all experiments.

The time factor was determined using Equation 6.13 obtained by rearranging Equation 6.5:

$$t = \frac{2}{t_f \psi}\left(\sqrt{1-\psi \ln(1-X)} - 1\right) \tag{6.13}$$

By plotting the real time, t, against $\sqrt{1-\psi\ln(1-X)}-1$, the time factor can be calculated from the slope, Δs_t, by inserting the regressed structural parameter value into this simplified relation:

$$t_f = \frac{2}{\psi \Delta s_t} \tag{6.14}$$

This was calculated for all the experiments.

The intrinsic reaction rate parameters were evaluated using Equations 6.8 and 6.12. Rearranging Equation 6.8 gives:

$$r_s = \frac{t_f(1-\varepsilon_o)}{S_o} \tag{6.15}$$

Equation 6.12 and Equation 6.15 are equal, since they define the same parameter, the intrinsic reaction rate, r_s, thus:

$$\frac{t_f(1-\varepsilon_o)}{S_o} = k_{so}\exp\left(\frac{-E_a}{RT}\right)y_{CO_2}^m \tag{6.16}$$

By defining a lumped pre-exponential factor, $k_{so}^{'}$:

$$k_{so}^{'} = \frac{k_{so}S_o}{(1-\varepsilon_{o)}} \tag{6.17}$$

Rearranging Equation 6.16:

$$t_f = k_{so}^{'}\exp\left(\frac{-E_a}{RT}\right)\cdot y_{CO_2}^m \tag{6.18}$$

And taking logarithms of both sides gives:

$$\ln(t_f) = -\frac{E_a}{RT} + m\ln(y_{CO_2}) + \ln(k'_{so}) \tag{6.19}$$

For kinetic parameter evaluations:

- Activation energy E_a, can be calculated using the slope of the plot of $\ln(t_f)$ against T^{-1} at constant CO_2 concentration.
- By plotting $\ln(t_f)$ against $\ln(y_{CO_2})$ at constant temperature, the reaction order with respect to CO_2 concentration *m*, can be determined from the slope.
- The lumped pre-exponential factor $\ln(k'_{so})$, can be evaluated from the intercepts of $\ln(t_f)$ against T^{-1} and $Ln(t_f)$ versus $\ln(y_{CO_2})$.

6.5 Evaluation of Kinetic Parameters

To effectively quantify the effect of the operational variables of the experiment: temperature; CO_2 composition in the reaction gas; and the different chars used, kinetic modelling using the random pore model (RPM) was conducted on all four chars. The evaluation of the RPM involves three steps (Kaitano, 2007; Everson *et al*., 2008;):

- The determination of the structural parameter ψ, through numerical regression of the experiment data using Equation 6.10;
- The calculation of the time scale parameter (time factor) t_f, which is one of the intrinsic reaction rate constants, for each of the experiments as outlined in Equations 6.13 and 6.14 using the structural parameter ψ, determined using Equation 6.10.;
- The evaluation of the other intrinsic reaction rate constants: activation energy E_a; reaction order *m*, with respect to CO_2 concentration in the reaction gas mixture; and the lumped pre-exponential factor, k'_{so}.

6.5.1 Evaluation of the Structural Factor, ψ

Equation 6.10 was used to determine the structural parameter.

$$\frac{t}{t_{0.9}} = \frac{\sqrt{1-\psi \ln(1-X)}-1}{\sqrt{1-\psi \ln(1-0.9)}-1} \tag{6.10}$$

The dimensionless time $t/t_{0.9}$ was calculated using the experimental real times *t*, at different carbon conversions *X*, and the time to reach 90% conversion, $t_{0.9}$. By choosing an initial arbitrary value for ψ; the term on the right hand side of Equation 6.10 was regressed numerically. Using the solver add-in function in Microsoft Excel, the value of ψ was iterated until the error sum of squares (ESS) converged to the lowest minimum using the equation:

$$ESS = \left[\left(\frac{t}{t_{0.9}}\right)_{Exp} - \left(\frac{\sqrt{1-\psi \ln(1-X)}-1}{\sqrt{1-\psi \ln(1-0.9)}-1}\right)_{Cal}\right]^2 \tag{6.20}$$

Note that the subscripts: *Exp* and *Cal* refer to reduced time determined from the experimental data and reduced time calculated using the arbitrary ψ values respectively.

The summary of this evaluation is given in Table 6.1, while the detailed results are included in Appendix C.

Table 6.1: Dimensionless structural parameters for the char pores.

Char ID	**Char B**	**Char C**	**Char C2**	**Char D2**
Structural Parameter, ψ (-)	1.11 ± 0.10	1.75 ± 0.18	2.58 ± 0.32	1.57 ± 0.20

Kaitano (2007) noted that the values of the structural parameter do not change significantly with variations of operating conditions. This was also observed with the char samples, as the respective ψ values for each experiment did not show substantial

variations to the average value for each of the chars. This is reflected in their acceptable average deviations which were: 9% for char B; 10% for char C; and 12% for both char C2 and D2 from their respective average values.

The structural parameter ψ, values for chars B, C and D2 were < 2. This shows that the maximum reaction rate and the maximum reactive surface area occur at the fractional carbon conversion, $X = 0$. Thus pore coalescence was more significant than pore growth at the initial stage of the reaction. From this point onwards, the reaction surface area and the reaction rate decreases with increasing conversion (Bhatia & Perlmutter, 1980).

For char C2 with a structural parameter value of 2.58, ($\psi > 2$), maximum reaction rate and maximum surface area do not occur at fractional carbon conversion $X = 0$ but at a latter value of X. This indicates that pore growth rather than pore coalescence is the initial dominant structural mechanism. Maximum reaction rate will thus occur when pore coalescence becomes more significant after the initial pore growth (Bhatia & Perlmutter, 1980, Liu *et al*., 2000; Kaitano, 2007). Apart from the ψ values, a good depiction of the significant structural mechanisms during the gasification reaction is the rate of reaction versus fractional conversion plots (Figure 5.5) presented in Section 5.5. It is clear from Figure 5.5, that except for char C2 with maximum rate of reaction occurring at about X = 0.2, implying that real time, t is > 0; chars B, C and D2 exhibited maximum rate of reaction at X = 0 and therefore, t = 0. These are similar to the findings and discussions of Bhatia & Perlmutter (1980); Liu *et al*. (2000); Kaitano (2007); Murillo *et al*. (2004 and 2006) and Everson *et al*. (2008a). Other results are given in Figure 6.8 of Section 6.6 and Appendices B and D. It is important to note that the char-CO_2 gasification reaction is sufficiently within Regime 1 (chemical reaction controlled), according to the RPM, not-withstanding the low porosity of the chars.

A comparison between the experimental results and the model predictions using a dimensionless plot of conversion X, against reduced time, $t/t_{0.9}$, for char B is presented in Figure 6.1. The result confirms that the evaluated structural parameter value is appropriate to describe the experimental data of char B. The dotted lines in the figure indicating the error interval. This was also validated for chars C, C2 and D2 with similar results and are included in Appendix C.

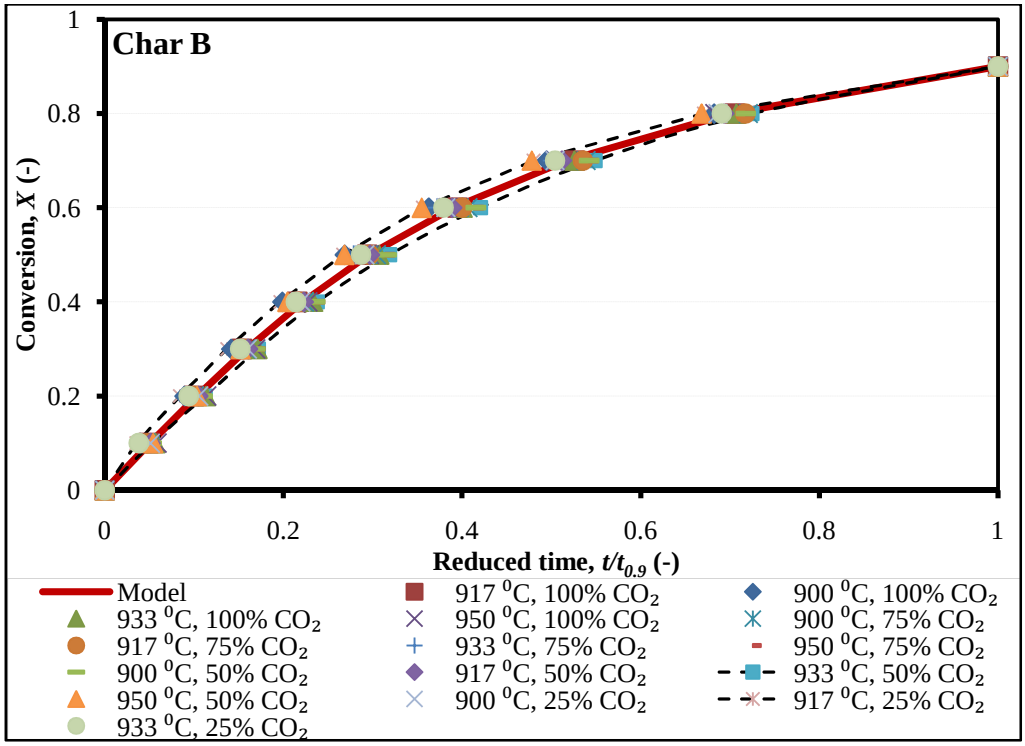

Figure 6.1: Comparison of the gasification experimental and model results for char B, 0.875 *bar*.

6.5.2 Determination of the Time Factor, t_f

The time scale parameter, the time factor (t_f), for all the experiments were determined using Equation 6.13 and 6.14.

$$t = \frac{2}{t_f \cdot \psi} \cdot \left(\sqrt{1-\psi \ln(1-X)} - 1\right) \tag{6.13}$$

$$t_f = \frac{2}{\psi \cdot \Delta s_t} \tag{6.14}$$

This was achieved by using the slope, Δs_t, of the plot of the experimental real times (t) versus the linearised function of X, $\left(\sqrt{1-\psi \ln(1-X)} - 1\right)$ and the evaluated structural parameter characteristic of the experiment. The time factor calculated at

various operating conditions, compared with the experimentally determined initial reactivity for char B as well as time taken to reach 50% and 90% conversion ($t_{0.5}$ and $t_{0.9}$), are summarised in Table 6.2. Similar results were obtained from corresponding evaluations for chars C, C2 and D2. These are presented in Appendix C.

Table 6.2: Summary of the structural parameter, time factors and initial reactivity for char B, 0.875 *bar*.

Temp. (℃)	y_{CO_2} (*mol. %)*	$t_{0.5}$ (*min*)	$t_{0.9}$ (*min*)	$R \cdot 10^{-3}$ (min^{-1})	$t_f \cdot 10^{-3}$ (min^{-1})	ψ (-)
900 ℃	25%	319.91	1099.2	1.56	1.51	1.06
917 ℃		231.10	866.13	2.16	1.97	0.91
933 ℃		198.93	693.10	2.51	2.38	1.03
950 ℃		143.47	484.65	3.49	3.35	1.11
900 ℃	50%	256.60	813.10	1.95	1.92	1.27
917 ℃		174.66	588.21	2.86	3.06	1.10
933 ℃		141.22	443.05	3.54	3.48	1.31
950 ℃		90.467	337.17	5.53	5.12	0.93
900 ℃	75%	223.57	735.65	2.24	2.13	1.21
917 ℃		162.97	549.93	3.07	2.87	1.17
933 ℃		101.53	364.33	4.92	4.57	1.02
950 ℃		74.417	237.13	6.72	6.59	1.26
900 ℃	100%	162.85	605.93	3.07	2.77	0.96
917 ℃		127.25	433.30	3.93	3.71	1.12
933 ℃		84.467	274.87	5.92	5.83	1.19
950 ℃		61.983	209.22	8.07	7.96	1.08

From the table, it is clear that the time factor increases with increasing temperature and CO_2 concentration, with values approximately equal to the experimentally determined initial reactivity of the chars. Similar results were reported by Kaitano (2007), for char gasification with CO_2. The time factor values obtained for chars B, C

and C2; as well as initial reactivity determined from the experimental data are close to each other, which suffices to say that their respective reactivity did not vary significantly as seen in Figure 5.17 of Section 5.7. Char D2 generally exhibited higher initial reactivity with a similar higher RPM determined time factor, t_f.

This confirms the correlation of char properties given earlier in Section 5.6. A closer look at Table 6.2 and a comparison of it with similar results (provided in Appendix C for chars C, C2 and D2) reveals and confirms further that the reactivity of char D2 is higher than the reactivity of the other three chars by a factor > 4. This is evident from their respective time factor and initial reactivity. This can also be deduced from the char comparison plots of Figure 5.17, Section 5.7.

6.5.3 Determination of Activation Energy, E_a

The activation energy of the chars was calculated using the linearised form of Equation 6.18 given in Equation 6.19:

$$\ln(t_f) = -\frac{E_a}{RT} + m\ln(y_{CO_2}) + \ln(k'_{so}) \tag{6.19}$$

This was achieved by plotting $\ln(t_f)$ against the reciprocal of the isothermal experimental temperature (in Kelvin), at constant CO_2 concentration. The apparent activation energy, E_a, was evaluated from the slope, Δs_{E_a}, according to the relation:

$$\Delta s_{E_a} = \frac{-E_a}{R} \tag{6.21}$$

A detailed result of the determined activation energy at different reaction gas mixtures for each of the four samples is presented in Table 6.3, while their respective Arrhenius plots, with correlation coefficients > 0.95, are shown in Figure 6.2.

Table 6.3: Details of results of activation energy for the char samples at different CO_2 concentrations in the reaction gas, 0.875 *bar*.

Char B			**Char C2**		
y_{CO_2} (mol.%)	E_a (kJ·mol^{-1})	R^2	y_{CO_2} (mol.%)	E_a (kJ·mol^{-1})	R^2
25%	185.4	0.987	25%	194.6	0.990
50%	221.5	0.966	50%	236.8	0.998
75%	276.2	0.991	75%	224.8	0.987
100%	259.5	0.990	100%	252.9	0.980
Average E_a, char B = 235.7 ± 32.2			**Average E_a, char C2 = 227.3 ± 17.6**		
Char C			**Char D2**		
25%	229.9	0.987	25%	152.3	0.974
50%	232.0	0.957	50%	168.1	0.990
75%	229.2	0.996	75%	165.0	0.973
100%	235.8	0.974	100%	167.7	0.995
Average E_a, char C = 231.7 ± 2.2			**Average E_a, char D2 = 163.3 ± 5.5**		

From the results it is clear that there are no significant variations in the activation energy of the chars at the various CO_2 gas mixtures. This is further corroborated by the small average deviations of 0.95%, 7.7%, and 3.3% respectively for chars C, C2 and D2. However, char B exhibited a relatively low activation energy value at 25% CO_2 concentration culminating in a rather higher average deviation of 13.6%.

The average activation energy values obtained for the chars are: 235.7 ± 32.2; 231.7 ± 2.2; 227.3 ± 17.6; and 163.3 ± 5.5 $kJ{\cdot}mol^{-1}$ for char B, C, C2 and D2 respectively. Thus, the activation energy for chars B, C and C2 are close to each other, while char D2 has the lowest E_a value. This may not be unconnected with the catalytic effect of the higher ash components of char D2 (Miura *et al*., 1989 and 1990; Sun *et al*., 2004; Zhang *et al*., 2006). The higher activation energy values for the other chars can be attributed to the high inertinite maceral content of the precursor coals (Sun *et al*., 2004). This leads to the formation of higher volumes of dense char carbon forms after pyrolysis, with poor burnout properties and longer residence time in gasification systems and other conversion processes (Kaitano, 2007; du Cann, 2008; Everson *et al*., 2008b).

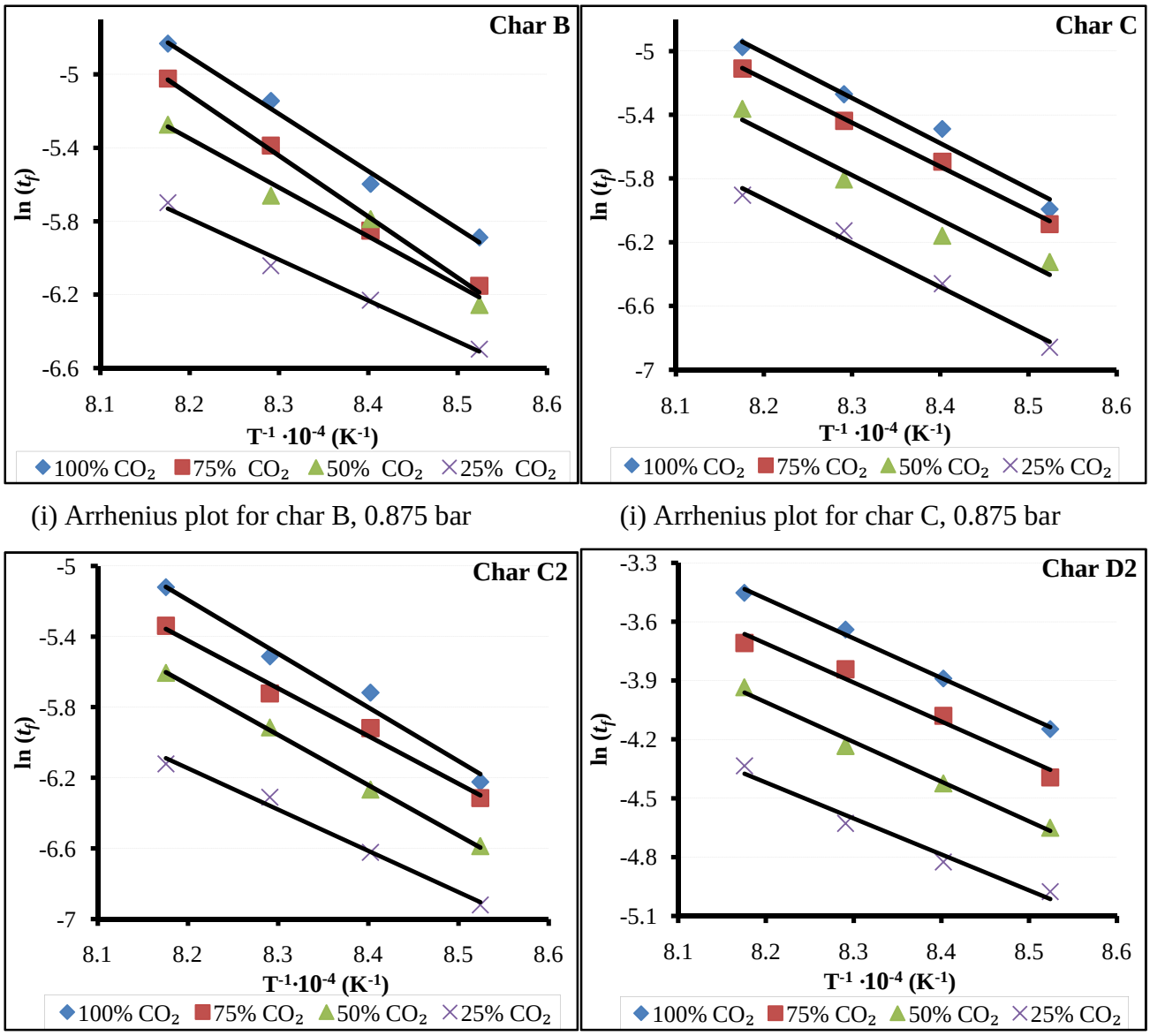

(i) Arrhenius plot for char B, 0.875 bar

(i) Arrhenius plot for char C, 0.875 bar

(iii) Arrhenius plot for char C2 at 0.875 *bar*

(iv) Arrhenius plot for char D2 at 0.875 *bar*

Figure 6.2: Arrhenius plots of the char-CO_2 gasification reaction at 100, 75, 50 and 25% CO_2 concentrations, 0.875 *bar*.

Activation energy values for CO_2 gasification of inertinite-rich chars of 199 - 266 $kJ{\cdot}mol^{-1}$ were reported by Kaitano (2007), while Everson *et al*. (2008a) observed E_a values of 192 - 247 $kJ{\cdot}mol^{-1}$ on similar chars (produced from inertinite-rich low grade coals). Comparison with other results from literature is presented in Table 6.7.

6.5.4 Determination of Order of Reaction, *m*

The reaction order *m*, with respect to CO_2 concentration in the reactant gas composition was determined using the linearised Equation 6.19. It was obtained directly from the slope of the plot of $Ln(t_f)$ versus $Ln(y_{CO_2})$ at constant temperature and pressure. This was determined for all the char samples.

$$\ln(t_f) = -\frac{E_a}{RT} + m\ln(y_{CO_2}) + \ln(k'_{so}) \qquad (6.19)$$

These plots are shown in Figures 6.3 and 6.4; while the evaluated order of reaction for all four chars including the correlation coefficient is presented in Table 6.4.

The results show that the orders of reaction of the char-CO_2 gasification with respect to CO_2 concentration are: 0.52 ± 0.11; 0.67 ± 0.03; 0.61 ± 0.07; and 0.63 ± 0.05 respectively for chars B, C, C2 and D2. The correlation coefficients for the plots are greater than 0.95. The average deviations for the determined order of reaction *m* of the chars are: 4.5% for char C; 11.5% for char C2; and 7.9% for chars D2. However, Char B exhibited a higher average deviation of 21%.

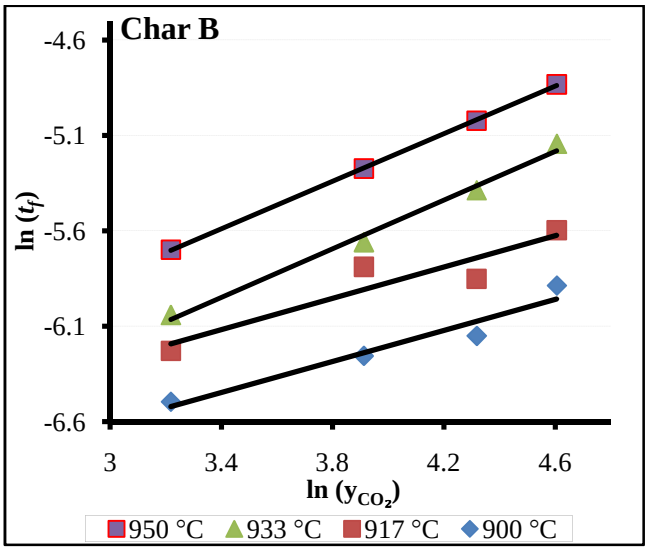

(i) Determination of gasification reaction order for char B

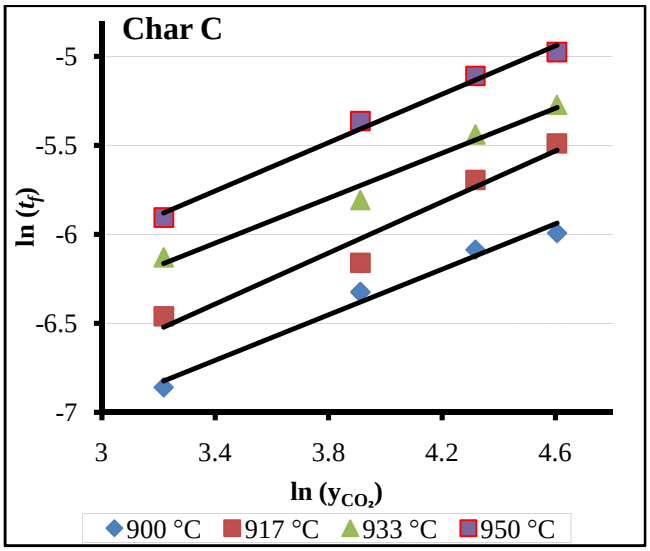

(i) Determination of gasification reaction order for char C

Figure 6.3: Determination of char-CO_2 gasification reaction order for chars B and C at various temperature and constant CO_2 concentrations, 0.875 *bar*.

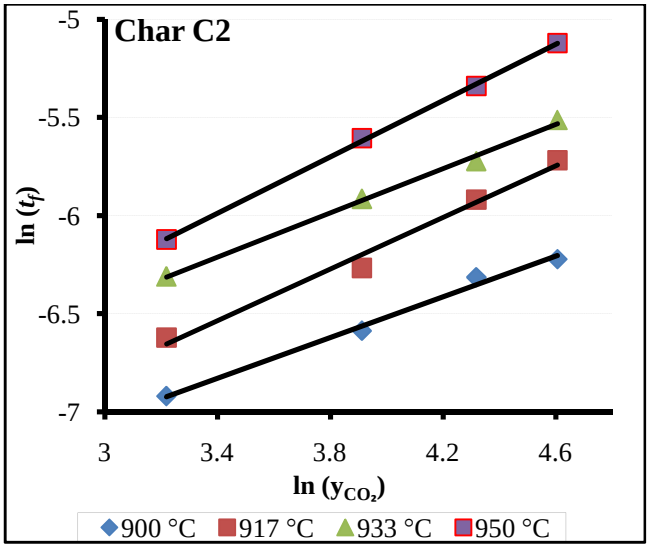

(i) Determination of gasification reaction order for char C2

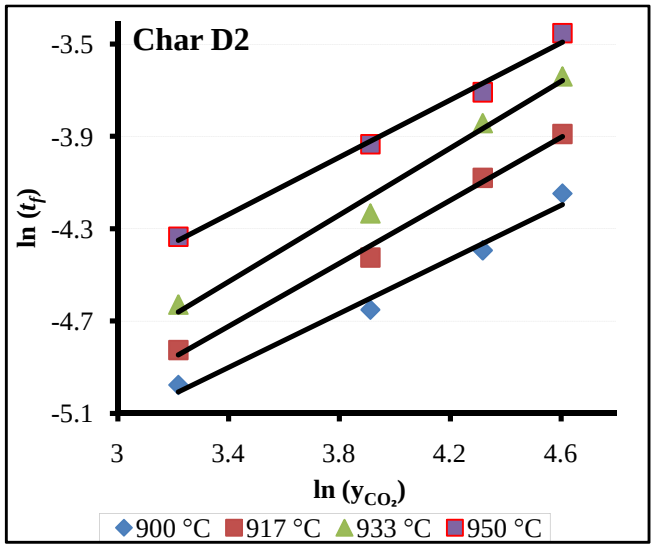

(i) Determination of gasification reaction order for char D2

Figure 6.4: Determination of char-CO_2 gasification reaction order for chars C2 and D2 at various temperature and constant CO_2 concentrations, 0.875 *bar*.

Table 6.4: Details of result for reaction order with respect to CO_2 concentration at different temperatures and constant CO_2 gas composition at 0.875 *bar*.

Char B			**Char C2**		
Temp. (℃)	$m\,(y_{CO_2}^m)$	R^2	Temp. (℃)	$m\,(y_{CO_2}^m)$	R^2
900 ℃	0.41	0.938	900 ℃	0.52	0.991
917 ℃	0.41	0.865	917 ℃	0.65	0.986
933 ℃	0.64	0.991	933 ℃	0.56	0.996
950 ℃	0.62	0.999	950 ℃	0.71	0.999
Average *m*: char B = 0.52 ± 0.11			**Average *m*: char C2 = 0.61 ± 0.07**		
Char C			**Char D2**		
900 ℃	0.64	0.980	900 ℃	0.57	0.989
917 ℃	0.71	0.956	917 ℃	0.59	0.982
933 ℃	0.63	0.979	933 ℃	0.72	0.987
950 ℃	0.68	0.990	950 ℃	0.62	0.991
Average *m*: char C = 0.67 ± 0.03			**Average *m*: char D2 = 0.63 ± 0.05**		

The order of char-CO_2 gasification reaction obtained in this study correlates well with the results of other investigators (Harris and Smith, 1990; Hampartsoumian *et al*., 1993; Fu and Wang, 2001; Ochoa *et al*., 2001; Kajitani *et al*., 2006). Comparison with published results from literature is also given in Table 6.7.

6.5.5 Determination of Lumped Pre-exponential Factor, k'_{so}

The lumped pre-exponential factor was determined from the intercepts of Figures 6.2 and 6.3 and 6.4. Details of the evaluation of k'_{so} at different CO_2 concentrations in the reaction gas mixture are given in Table 6.5. From the results, average lumped pre-exponential factor values of: $5.22 \pm 2.0 \cdot 10^8$; $4.36 \pm 1.9 \cdot 10^7$; $1.12 \pm 1 \cdot 10^8$; and $2.69 \pm 1 \cdot 10^5$ $min^{-1} \cdot bar^{-1}$ were obtained for char B, C, C2 and D2 respectively. This range of results is in good agreement with results reported by Miura *et al*., (1990); Fu and Wang, (2001); Kaitano, (2007); Everson *et al*., (2008a); and Sangtong-Ngam and Narasingha, (2008).

Table 6.5: Determination of lumped pre-exponential factor for the four char samples, 0.875 *bar*.

Char B		**Char C2**	
y_{CO_2}	k'_{so} ($min^{-1} \cdot bar^{-1}$)	y_{CO_2}	k'_{so} ($min^{-1} \cdot bar^{-1}$)
25%	$1.07 \cdot 10^8$	25%	$9.25 \cdot 10^6$
50%	$4.62 \cdot 10^8$	50%	$4.77 \cdot 10^7$
75%	$5.53 \cdot 10^8$	75%	$1.86 \cdot 10^7$
100%	$9.67 \cdot 10^8$	100%	$3.74 \cdot 10^8$
Average k'_{so} = 5.22 ± 2.0 ·10^8		**Average k'_{so} = 1.12 ± 1.0·10^8**	
Char C		**Char D2**	
25%	$1.86 \cdot 10^7$	25%	$4.01 \cdot 10^4$
50%	$3.53 \cdot 10^7$	50%	$2.88 \cdot 10^5$
75%	$3.71 \cdot 10^7$	75%	$2.85 \cdot 10^5$
100%	$8.35 \cdot 10^7$	100%	$4.65 \cdot 10^5$
Average k'_{so} = 4.36 ± 1.9 ·10^7		**Average k'_{so} = 2.69 ±1.0 ·10^5**	

A summary of the structural and kinetic parameters derived from this study is presented in Table 6.6, while a comparison with published results from other investigators is presented in Table 6.7.

Table 6.6: Summary of structural and kinetic parameters for chars B, C, C2 and D2.

Kinetic Parameter	Char B	Char C	Char C2	Char D2
ψ (-)	1.11 ± 0.10	1.75 ± 0.18	2.58 ± 0.32	1.57 ± 0.20
m (-)	0.52 ± 0.11	0.67 ± 0.03	0.61 ± 0.07	0.63 ± 0.05
E_a, (kJ·mol^{-1})	235.7 ± 32.2	231.7 ± 2.2	227.3 ± 17.6	163.3 ± 5.5
k'_{so}, (min^{-1}·bar^{-1})	5.22 ± 2.0 ·10^{8}	4.36 ± 1.9 ·10^{7}	1.12 ± 1.0·10^{8}	2.69 ±1 ·10^{5}

6.6 Validation of Kinetic Model and Associated Parameters

The validation of the RPM was done by a plot of experimental or actual initial reactivity, R, versus the RPM predicted initial reactivity designated by the time scale parameter (time factor), t_f. The relationship between the actual- and predicted t_f for all four chars is shown in the parity plot of Figure 6.5.

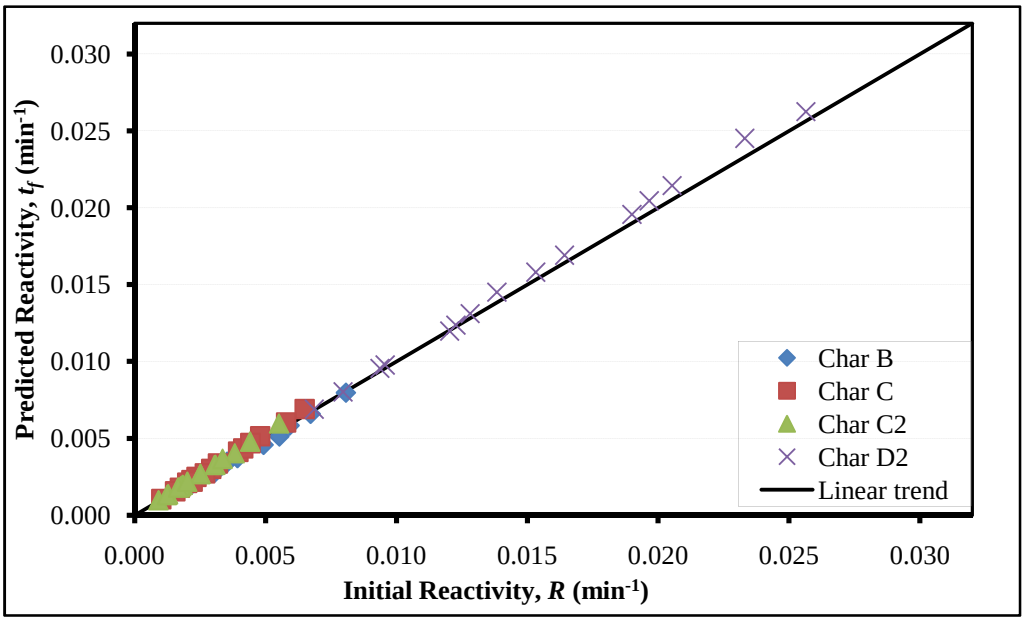

Figure 6.5: Parity plot of predicted versus actual t_f values for all four char samples.

Table 6.7: Models used, structural parameter, and kinetic parameters obtained for char-CO_2 gasification reaction by other investigators.

Parent coal type	Reactor used	Temperature range (°C)	Model used	ψ (-)	E_a (kJ·mol^{-1})	m (-)	k'_{so} (min^{-1}·bar^{-1})	Reference
Bituminous	TGA	900-950	RPM	1.11-2.58	163-236	0.52-0.67	$2.69\cdot10^{5}$-$5.22\cdot10^{8}$	This investigation
Lignite	TGA	840-1100	VRM	-	248	-	-	Dutta *et al*., 1977
Sub bituminous	TGA	800-950	SCM	-	109-137	-	-	Everson *et al*., 2006
Coal discard	TGA	850-900	RPM	1.04	192-247	-	$8.69\cdot10^{7}$-$1.03\cdot10^{8}$	Everson *et al*., 2008a
Coal	TGA	927-1127	SUCM	-	245	0.85	$1.18\cdot10^{7}$	Fu and Wang, 2001
UK coals	EFR	627-960	-	-	239	0.5-0.6	-	Hampartsoumian *et al*., 1993
Brown coal	VTR	750-900	-	-	214-230	0.57	-	Harris and Smith, 1990
Bituminous	HPTGA	900-1000	RPM	1.23-1.43	171-202	0.49-0.77	-	Hattingh, 2009
Coal discard	HPTGA	850-900	RPM	1.04	192-266	0.5	$9.60\cdot10^{8}$	Kaitano, 2007
Bituminous	PDTF/TGA	750-1400	RPM	1.0-26	240-280	0.43-0.56	$2.54\cdot10^{7}$-$1.19\cdot10^{9}$	Kajitani *et al*., 2006
Sub bituminous	TGA	885-985	VRM	-	268	-	-	Matsui *et al*., 1987
Lignite	TGA	650-900	Various	5.0[a]	204-212	0.71-1.0	$1.45\cdot10^{3}$-$6.17\cdot10^{6}$	Murillo *et al*., 2006
Sub bituminous	TGA	900-1160	RPM	4.7-7.0	156-165	0.50-0.58	-	Ochoa *et al*., 2001
UK coal	TGA	827-1102	-	-	220	-	-	Radovic *et al*., 1985
Lignite	HTR	900-980	-	-	128-146	-	-	Sinağ *et al*., 2003
Anthracites	TGA	920-1050	SCM	-	146-202	-	$9.2\cdot10^{3}$-$9.8\cdot10^{5}$	Zhang *et al*., 2006

[a]- Determined using RPM

From the parity plot, it is obvious that the predicted initial reactivity of the chars by the RPM time factor, (t_f) is a good approximation of the experimentally determined initial reactivity. This is good evidence to uphold the validity of the RPM to describe the char-CO_2 gasification reaction with respect to this investigation under Regime I.

The validity of the model was also checked by constructing a plot of the experimentally determined conversions with the RPM predicted conversions. This is demonstrated in Figure 6.6 for char B at all the experimental conditions at 0.875 *bar* pressure. The results obtained for char C, C2 and D2 compare very well with the results of char B and can be found in Appendix C.

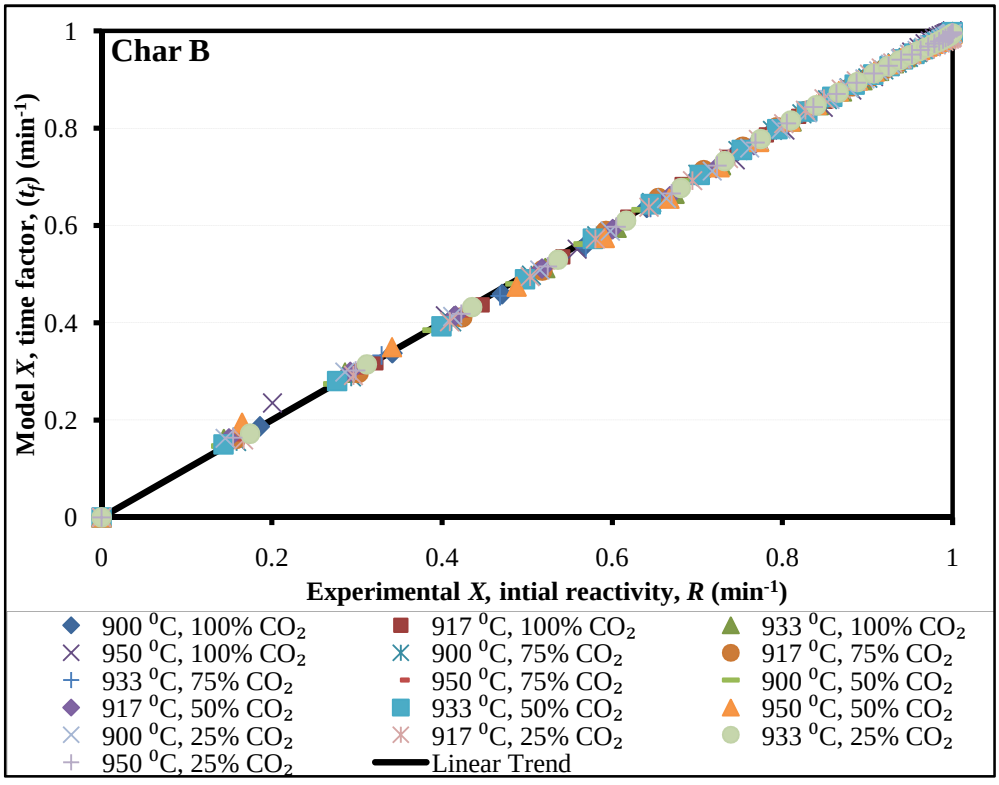

Figure 6.6: Comparison between experimental and model gasification results for char B.

The fitting of the RPM to the experimental conversion data for all four char samples was conducted as a further validation of the model. The results of this fitting at different operating conditions are given in Figure 6.7(i) - (iv). It can be observed from the results that the RPM adequately described the experimental data (conversion) of all four chars under Regime I. Only part of the results is presented in Figure 6.7, while the remainder are included in Appendix D.

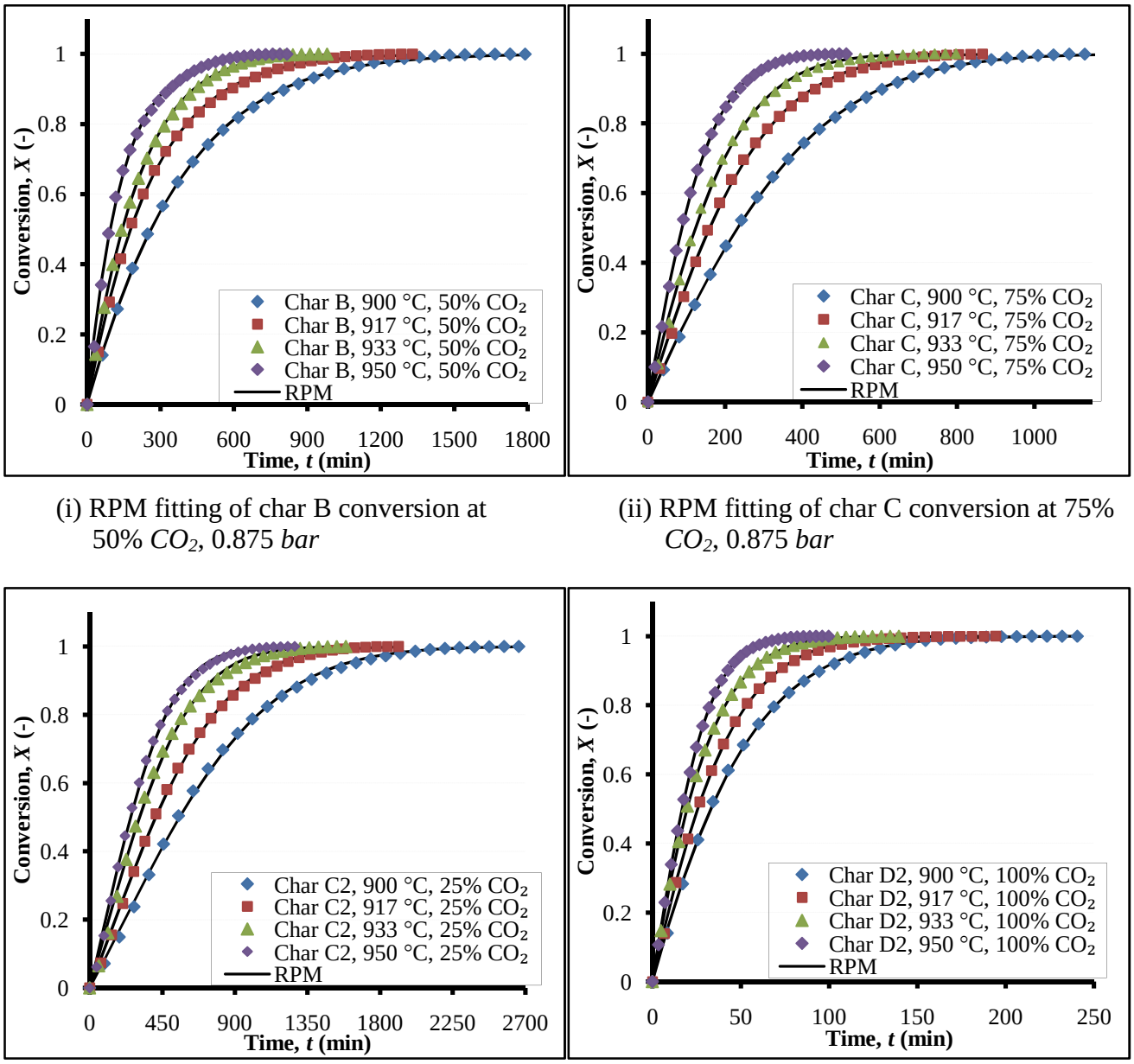

(i) RPM fitting of char B conversion at 50% CO_2, 0.875 *bar*

(ii) RPM fitting of char C conversion at 75% CO_2, 0.875 *bar*

(iii) RPM fitting of char C2 conversion at 25% CO_2, 0.875 *bar*

(iv) RPM fitting of char C2 conversion at 100% CO_2, 0.875 *bar*

Figure 6.7: RPM fitting of char conversion at different CO_2 concentrations.

It was also possible to use the RPM to predict the rate of reaction. Fittings of the RPM predicted conversion rate (d*X*/d*t*) versus fractional conversion to the experimental reaction rate change against fractional conversion were constructed and are presented in Figure 6.8. Again, a good fit was obtained. More of these plots are provided in Appendix D.

The good fit to the experimental data exhibited by RPM is a good confirmation of the validity of the model and also shows that the gasification reaction is under Regime I (chemical reaction controlled).

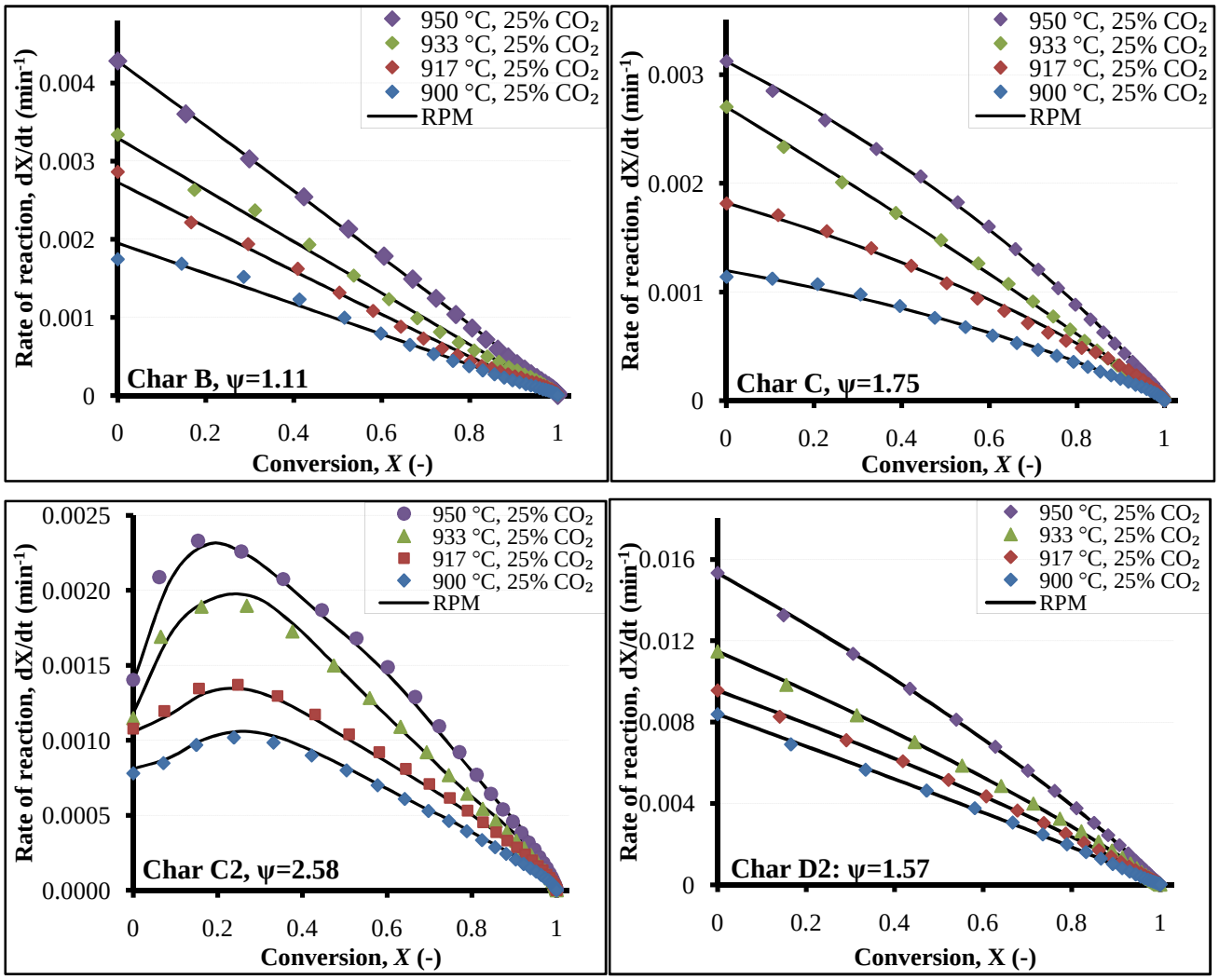

Figure 6.8: RPM fitting of char conversion rate for chars B, C, C2 and D2 at 25% CO_2 concentration and different temperatures.

6.7 Summary

Structural parameters, ψ, determined for chars B, C, C2 and D2 are 1.11, 1.75, 2.58 and 1.57 respectively. This shows that the maximum reaction rate and maximum reaction surface area occur at $X = 0$ for chars B, C, and D2 and at: $X > 0$ for char C2 (Bhatia and Perlmutter, 1980; Liu *et al*., 2000; Kaitano, 2007). Pore coalescence was therefore the dominant structural mechanism during the initial stage of gasification for chars B, C and C2. On the other hand, pore growth was more significant for char C2 during the initial period of the gasification reaction. This was corroborated by the conversion plots of the chars and validated by the satisfactory correlation in the plot of experimental conversion against the reduced time ($t/t_{0.9}$) for each experiment.

The time scale parameter, t_f, determined for each experiment were similar in value to the initial reactivity evaluated from the experimental result. The RPM predicted reactivity also confirmed the higher reactivity of the chars, with the reactivity of char D2 higher than that of the other chars by a factor > 4. The time factor was validated by a parity plot of model predicted initial reactivity (t_f) versus the experimentally determined reactivity *R*. This showed a consistent linear trend for all four chars.

The activation energy obtained for the gasification reactions are: 235.7 $kJ{\cdot}mol^{-1}$ for char B; 231.7 $kJ{\cdot}mol^{-1}$ for char C; 227.3 $kJ{\cdot}mol^{-1}$for char C2; and 163.3 $kJ{\cdot}mol^{-1}$ for char D. The order of reaction with respect to CO_2 concentration in the reaction gas composition were found to be between 0.52 to 0.67 for the chars. Lumped pre-exponential factors stood at: 5.22 $\cdot 10^8$; 4.36 $\cdot 10^7$; 1.12 $\cdot 10^8$; and 2.69 $\cdot 10^5$ $min^{-1}bar^{-1}$ for chars B, C, C2, and D2 respectively. The lower activation energy of char D2 was attributed to its lower rank with respect to the other chars and the significant catalytic influence of inorganic components of the ash.

The random pore model (RPM) was found to satisfactorily describe the experimental results of chars B, C, C2 and D2 in the reaction controlled regime (Regime I). The RPM was validated by a parity plot of the experimental conversion against the model predicted conversion which followed a linear trend for the four chars. The fitting of the RPM conversions and conversion rates data to the experimental conversions and conversion rates also gave adequate fits.

The kinetic parameters and the reaction rate constants determined for each char corresponded well with published results in the open literature.

The intrinsic reaction rate of the chars can thus be written in these empirical Arrhenius forms:

Char B: $$r_s = 5.22\times10^{8}\cdot\exp\left(\frac{-235700}{RT}\right)\cdot\left(y_{CO_2}\right)^{0.52} \quad (6.22)$$

Char C: $$r_s = 4.36\times10^{7}\cdot\exp\left(\frac{-231700}{RT}\right)\cdot\left(y_{CO_2}\right)^{0.67} \quad (6.23)$$

Char C2: $$r_s = 1.12\times10^{8}\cdot\exp\left(\frac{-227300}{RT}\right)\cdot\left(y_{CO_2}\right)^{0.61} \quad (6.24)$$

Char D2: $$r_s = 2.69\times10^{5}\cdot\exp\left(\frac{-163300}{RT}\right)\cdot\left(y_{CO_2}\right)^{0.63} \quad (6.25)$$